MPP-2003-123
LPHEA-03-09
hep-ph/0311149

Radiative corrections to scalar-fermion pair production in high energy e^+e^- collisions

A. Arhrib[1,2,3], W. Hollik[1*]

1: Max-Planck-Institut für Physik (Werner-Heisenberg-Institut)
Föhringer Ring 6, D–80805 Munich, Germany

2: Département de Mathématiques, Faculté des Sciences et Techniques
B.P 416 Tanger, Morocco.
and
LPHEA, Département de Physique, Faculté des Sciences-Semlalia,
B.P. 2390 Marrakesh, Morocco.

3: The Abdus Salam ICTP, P.O. Box 586, 34100 Trieste, Italy.

Abstract

We study the one-loop radiative corrections to pair production of the supersymmetric scalar partners of the standard fermions in e^+e^- annihilation. Both electroweak and SUSY-QCD corrections are considered. Applications are for production of scalar fermions of the third generation, $e^+e^- \to \tilde{f}_i\tilde{f}_j^*$ (i,j=1,2), $f = t, b, \tau$, as well as for production of scalar quarks of the first and second generation. Effects on integrated cross sections are discussed and also the one-loop induced forward-backward asymmetries are studied. It is found that at low energy, $\sqrt{s} \approx 500 \to 1000$ GeV, the corrections are dominated by the QCD contributions, At high energy, $\sqrt{s} \geq 2$ TeV, the electroweak box diagrams give a substantial contribution and even dominate in some regions of parameters space. The purely loop-induced forward-backward asymmetry can reach values of several per cent.

*E-mail: arhrib@mppmu.mpg.de, hollik@mppmu.mpg.de

1 Introduction

Supersymmetry is one of the most promising extensions of the Standard Model (SM), and the Minimal Supersymmetric Standard Model (MSSM) is the popular scenario of realization of Supersymmetry [1]. The MSSM predicts the existence of scalar partners to all known quarks and leptons. Since SUSY is broken, these particles can have masses larger than the masses of their standard partners; however, naturalness arguments suggest that the scale of SUSY breaking, and hence the masses of the SUSY particles should not exceed $\mathcal{O}$(1TeV). In Grand Unified SUSY models, the third generation of scalar fermions, $\widetilde{t}, \widetilde{b}, \widetilde{\tau}$, gets a special status; due to the influence of Yukawa-coupling evolution, the scalar fermions of the third generation are expected to be lighter than the scalar fermions of the first and second generations.

Scalar quarks can be produced copiously both at hadron and lepton colliders. So far, the search for SUSY particles at colliders has not been successful, and under some assumptions on the decay rates, one can only set lower limits on their masses. CDF excludes scalar quarks of the first and second generations with masses lower than $\mathcal{O}$(250 GeV) [2], while for scalar top and scalar bottom the bounds are lower. LEP experiments also searched for scalar fermions, depending on assumptions on the Lightest Supersymmetric Particle (LSP); the results can be summarized as follows [3]:

- from $e^+e^- \to \widetilde{t}_1\widetilde{t}_1$, and assuming that the splitting $m_{\widetilde{t}_1} - m_{LSP} \geq 10$ GeV :
  i) if the stop decays as $\widetilde{t}_1 \to c\widetilde{\chi}_1^0$, the lower limit on the $\widetilde{t}$ mass is 97.6 (95.7) GeV for stop mixing $\widetilde{\theta}_t = 0$ ($\widetilde{\theta}_t = 0.98$).
  ii) if the stop decays as $\widetilde{t}_1 \to bl\widetilde{\nu}$, $l = e, \mu, \tau$, the lower limit is 96 (92.6) GeV for stop mixing $\widetilde{\theta}_t = 0$ ($\widetilde{\theta}_t = 0.98$).
  iii) if the stop decays as $\widetilde{t}_1 \to b\tau\widetilde{\nu}_\tau$ with 100% branching ratio, the lower limit is 95.5 (91.5) GeV for stop mixing $\widetilde{\theta}_t = 0$ ($\widetilde{\theta}_t = 0.98$).

- from $e^+e^- \to \widetilde{b}_1\widetilde{b}_1$ followed by the decay $\widetilde{b}_1 \to b\widetilde{\chi}_1^0$ and assuming for the splitting $m_{\widetilde{b}_1} - m_{LSP} \geq 10$ GeV, the lower limit on the $\widetilde{b}$ mass is 96.9 (85.1) GeV for sbottom mixing $\widetilde{\theta}_b = 0$ ($\widetilde{\theta}_b = 1.17$).

Note that a mixing scenario with $\widetilde{\theta}_t = 0.98$ ($\widetilde{\theta}_b = 1.17$) corresponds to the case where the light scalar top decouples from the Z boson, with the $Z\widetilde{t}_1\widetilde{t}_1^*$ coupling ≈ 0 (or the light scalar bottom decouples from Z boson, with the $Z\widetilde{b}_1\widetilde{b}_1^*$ coupling ≈ 0, respectively).

Higher-energy hadron and e^+e^- colliders of the next generation will be required to sweep the entire mass range, up to $\mathcal{O}$ (1TeV), for the supersymmetric particles. If SUSY particles would be detected at hadron colliders, their properties can be studied with high accuracy at a high-energy linear e^+e^- collider [4]. It has been shown that the expected experimental precision for slepton-mass measurements is of the order of 100 MeV [4]. It is thus mandatory to incorporate effects beyond leading order into the theoretical predictions in order to match the experimental accuracy. In particular, QCD corrections to squark-pair production have to be included. The next-to-leading order corrections to squark-pair

production at proton colliders have been studied in [5] and found to increase the cross section.

For e^+e^- machines, scalar-fermion production has been addressed in several studies and shown to be promising for precision analysis of sfermion properties with mass and mixing-angle reconstructions [4, 6]. QCD corrections to squark-pair production were shown, a decade ago, to be large [7, 8, 9], and the gluino contributions [8, 9] were found to be rather small. Gluon emission from scalar quarks has been studied in [10]. On the electroweak side, for squark and slepton production in e^+e^- annihilation the leading and subleading electroweak Sudakov logarithms were investigated [11, 12] and found to be large at high energy. Recently, the full one-loop radiative corrections to the production of scalar muons and scalar electrons have been presented in [13], and in refs [13, 14], it was shown that near threshold important corrections to the cross section arise from Coulomb corrections and finite slepton widths. A few years ago, a part of the Yukawa corrections (the one associated with vertex corrections) to the third generation of scalar fermions was considered in [15].

In this paper we provide the complete result for the electroweak corrections to scalar-fermion pair production in e^+e^- annihilation, including self energies, vertex corrections, box diagrams, and real photon emission, and discuss their effects in combination with the QCD corrections. As applications, we focus on two types of observables: total cross sections and forward–backward asymmetries, the latter one being purely loop-induced.

The paper is organized as follows. In the next section, we will first set the notations and give the tree-level results. Section 3 outlines the calculation and the renormalization scheme. In section 4 we will discuss the effects of radiative corrections for various types of sfermions, with a short conclusion in section 5.

2 Notation and tree-level results

First we summarize the MSSM parameters entering our analysis, with particular attention to the sfermion sector. In the MSSM, the sfermion sector is specified by the mass matrix in the basis $(\tilde{f}_L, \tilde{f}_R)$. In terms of the scalar masses $\widetilde{M}_L$, $\widetilde{M}_R$, the Higgs-Higgsino mass parameter μ, and the soft SUSY-breaking trilinear couplings A_f, the sfermion squared-mass matrices are given by [16]

$$\mathcal{M}^2_{\tilde{f}} = \begin{pmatrix} m_f^2 + m_{LL}^2 & m_{LR} m_f \\ m_{LR} m_f & m_f^2 + m_{RR}^2 \end{pmatrix} \tag{2.1}$$

with

$$m_{LL}^2 = \widetilde{M}_L^2 + m_Z^2 \cos 2\beta \, (I_3^f - Q_f s_W^2), \tag{2.2}$$

$$m_{RR}^2 = \widetilde{M}_R^2 + m_Z^2 \cos 2\beta \, Q_f s_W^2, \tag{2.3}$$

$$m_{LR} = A_f - \mu \, (\tan\beta)^{-2I_3^f} \, . \tag{2.4}$$

$I_3^f = \pm 1/2$ and Q_f are the weak isospin and the electric charge of the sfermion $\tilde{f}$, and $\tan\beta = v_2/v_1$ with the vacuum expectation values of the Higgs fields, v_1 and v_2.

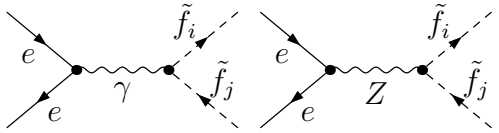

D_1 D_2

Figure 1: Tree level contribution to $e^+e^- \to \widetilde{f}_i\widetilde{f}_j^*$, with momenta $k_1(e^-)$, $k_2(e^+)$, $k_3(\widetilde{f}_i)$.

The hermitian matrix (2.1) is diagonalized by a unitarity matrix $R^{\tilde{f}}$, which rotates the current eigenstates, $\tilde{f}_L$ and $\tilde{f}_R$, into the mass eigenstates $\tilde{f}_1$ and $\tilde{f}_2$ as follows,

$$\begin{pmatrix} \tilde{f}_1 \\ \tilde{f}_2 \end{pmatrix} = R^{\tilde{f}} \begin{pmatrix} \tilde{f}_L \\ \tilde{f}_R \end{pmatrix} = \begin{pmatrix} \cos\widetilde{\theta}_f & \sin\widetilde{\theta}_f \\ -\sin\widetilde{\theta}_f & \cos\widetilde{\theta}_f \end{pmatrix} \begin{pmatrix} \tilde{f}_L \\ \tilde{f}_R \end{pmatrix} , \tag{2.5}$$

yielding the physical mass eigenvalues, with the convention $m_{\tilde{f}_1} < m_{\tilde{f}_2}$,

$$m^2_{\tilde{f}_{1,2}} \;=\; \frac{1}{2}(2m_f^2 + m_{LL}^2 + m_{RR}^2 \mp \sqrt{(m_{LL}^2 - m_{RR}^2)^2 + 4m_{LR}^2 m_f^2}) \; . \tag{2.6}$$

The mixing angle $\widetilde{\theta}_f$ obeys the relation

$$\tan 2\widetilde{\theta}_f = \frac{2m_{LR}m_f}{m_{LL}^2 - m_{RR}^2} \quad . \tag{2.7}$$

Hence, for the case of the supersymmetric partners of the light fermions, L–R mixing can be neglected. However, mixing between top squarks can be sizable and allows one of the two mass eigenstates to be lighter than the top quark. Bottom-squark and τ-slepton mixing can also be significant if $\tan\beta$ is large.

The interaction of the neutral gauge bosons γ and Z with the sfermion-mass eigenstates is described by the Lagrangian

$$\mathcal{L} = \quad -ieA^\mu \sum_{i=1,2} Q_f \tilde{f}_i^* \overleftrightarrow{\partial}_\mu \tilde{f}_i + iZ^\mu \sum_{i,j=1,2} g_{Z\widetilde{f}_i\widetilde{f}_j} \tilde{f}_i^* \overleftrightarrow{\partial}_\mu \tilde{f}_j \tag{2.8}$$

with the couplings

$$g_{Z\widetilde{f}_i\widetilde{f}_j} = -\frac{e}{s_W c_W}\{(I_3^f - Q_f s_W^2)R_{j1}^{\widetilde{f}} R_{i1}^{\widetilde{f}} - Q_f s_W^2 R_{j2}^{\widetilde{f}} R_{i2}^{\widetilde{f}}\} \tag{2.9}$$

involving the matrix $R^{\tilde{f}}$ from the transformation (2.5).

Neglecting the electron–Higgs coupling, the production of sfermion pairs in e^+e^- collisions proceeds in lowest order through s-channel photon and Z boson exchanges (Fig. 1). The tree level amplitude can be written as follows,

$$\mathcal{M}^0 = \mathcal{M}_L^0 \; I_L + \mathcal{M}_R^0 \; I_R \quad \text{with} \quad I_{L,R} = \bar{v}(k_1) \; \not{k}_3 \frac{1 \mp \gamma_5}{2} u(k_2) \tag{2.10}$$

and with

$$\mathcal{M}^0_{L,R} \;=\; 2e^2(-\delta_{ij}\frac{Q_f}{s} + \frac{g_{L,R}\, g_{Z\widetilde{f}_i\widetilde{f}_j}}{(s-M_Z^2)})\,, \tag{2.11}$$

where

$$g_L = \frac{1-2s_W^2}{2s_W c_W} \qquad , \qquad g_R = \frac{-2s_W^2}{2s_W c_W}\,. \tag{2.12}$$

The angular distribution for the production of a pair of sfermions $\widetilde{f}_i$, $\widetilde{f}_j^*$ is given by

$$\frac{d\sigma_0}{d\Omega} = N_C \frac{s\kappa_{ij}^3}{1024\pi^2}(|\mathcal{M}^0_L|^2 + |\mathcal{M}^0_R|^2)\sin^2\theta\,, \tag{2.13}$$

where $N_C = 3$ (1) for scalar quarks (scalar leptons). $\sqrt{s}$ is the CMS energy, θ the CMS scattering angle between e^+ and $\widetilde{f}_i$, and κ_{ij} the final-sfermion velocity,

$$\kappa_{ij}^2 = (1-\mu_i^2-\mu_j^2)^2 - 4\mu_i^2\mu_j^2 \quad , \quad \mu_{i,j}^2 = \frac{m^2_{\widetilde{f}_{i,j}}}{s}\,. \tag{2.14}$$

Angular integration yields the total cross section,

$$\sigma_0 = N_C \frac{s\kappa_{ij}^3}{384\pi}(|\mathcal{M}^0_L|^2 + |\mathcal{M}^0_R|^2)\,. \tag{2.15}$$

The angular distribution (2.13) is symmetric, and hence it is obvious that the forward–backward asymmetry A_{FB}, defined by

$$A_{FB} = \frac{\int_{\theta\le\pi/2} d\Omega \frac{d\sigma}{d\Omega} - \int_{\theta\ge\pi/2} d\Omega \frac{d\sigma}{d\Omega}}{\int_{\theta\le\pi/2} d\Omega \frac{d\sigma}{d\Omega} + \int_{\theta\ge\pi/2} d\Omega \frac{d\sigma}{d\Omega}} = \frac{\sigma_F - \sigma_B}{\sigma}\,, \tag{2.16}$$

vanishes in lowest order. The quantum corrections, however, in particular the box diagrams, contribute to $A_{FB} \neq 0$.

3 Structure of radiative corrections

3.1 One-loop diagrams for $e^+e^- \to \widetilde{f}_i\widetilde{f}_j^*$

The Feynman diagrams for the one-loop virtual contributions are generically displayed in Figures 2 – 5. These comprise the corrections to photon and Z propagators and their mixing (Fig. 2), the corrections to the initial-state vertices $\{\gamma, Z\}e^+e^-$, the corrections to the final-state vertices $\{\gamma, Z\}\widetilde{f}_i\widetilde{f}_j^*$ (Fig. 3), and the box contributions (Fig. 4).[1] These diagrams are to be supplemented by the external self-energy contributions for $e^\pm$ and scalar

[1] In this terminology, diagrams with irreducible one-loop 4-point (3-point) functions are labeled as box diagrams (vertex corrections)

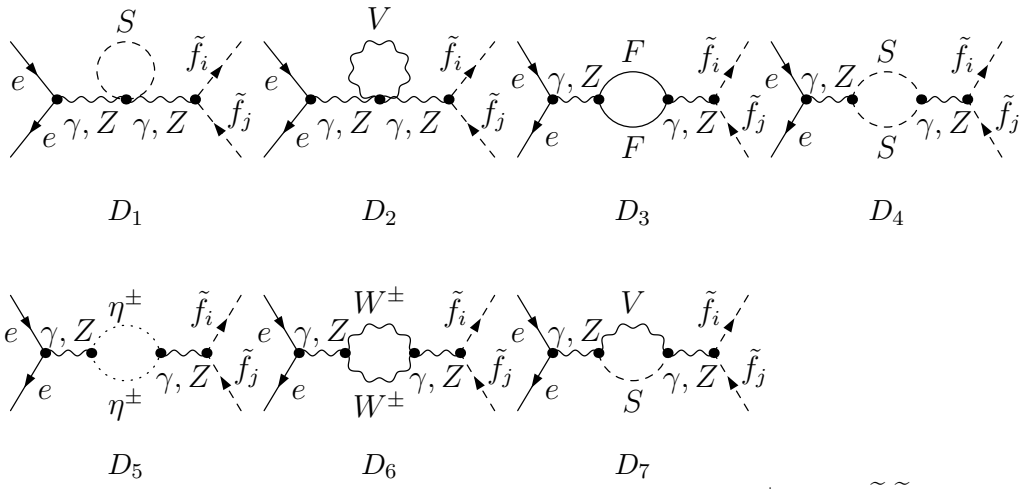

Figure 2: One–loop self–energy contributions to $e^+e^- \to \widetilde{f}_i \widetilde{f}_j^*$

fermions $\widetilde{f}_{i,j}$, which are part of the counterterms for propagators and vertices (Fig. 5), to be added according to renormalization. In the generic notation, V, S, F denote all insertions of vector, scalar, and fermionic states.

Note that loop contributions coming from initial state $e^+e^-H_0$ and $e^+e^-h_0$ vertices vanish for $m_e \to 0$ since e^+ and e^- are both on-shell. A similar argument holds for the A^0 and neutral Goldstone-boson exchange diagrams.

The Feynman diagrams are generated and evaluated using the packages FeynArts and FormCalc [17]. We have also used LoopTools and FF [18] in the numerical analysis.

The one-loop amplitudes are ultraviolet (UV) and infrared (IR) divergent. The UV singularities are treated by dimensional reduction [19] and are compensated in the on-shell renormalization scheme. We have checked explicitly that the results are identical in using dimensional reduction and dimensional regularization. The IR singularities are regularized with a small fictitious photon mass δ.

Diagrams like $D_{5,9}$ of Fig. 3 and diagrams $D_{6,8}$ of Fig. 4 and $D_{1\ldots4}$ of Fig. 5 are IR divergent when the exchanged gauge boson is a photon. For an IR-finite cross section we have to add the contribution from real-photon emission, $e^+e^- \to \widetilde{f}_i \widetilde{f}_j^* \gamma$. We limit ourself to the soft photon approximation where a cut ΔE on the energy of the photon is introduced. This approach have been used also for charged Higgs pair production in [20, 21].

It is interesting to note that the subclass of virtual and real photonic corrections is UV finite and does not require renormalization of any parameters. UV divergences from virtual photons cancel between vertex corrections and external wave-function renormalizations. The photonic corrections are thus completely determined by the gauge couplings, as already present in the Born approximation, and can be separately considered as (cut-dependent) "QED corrections".

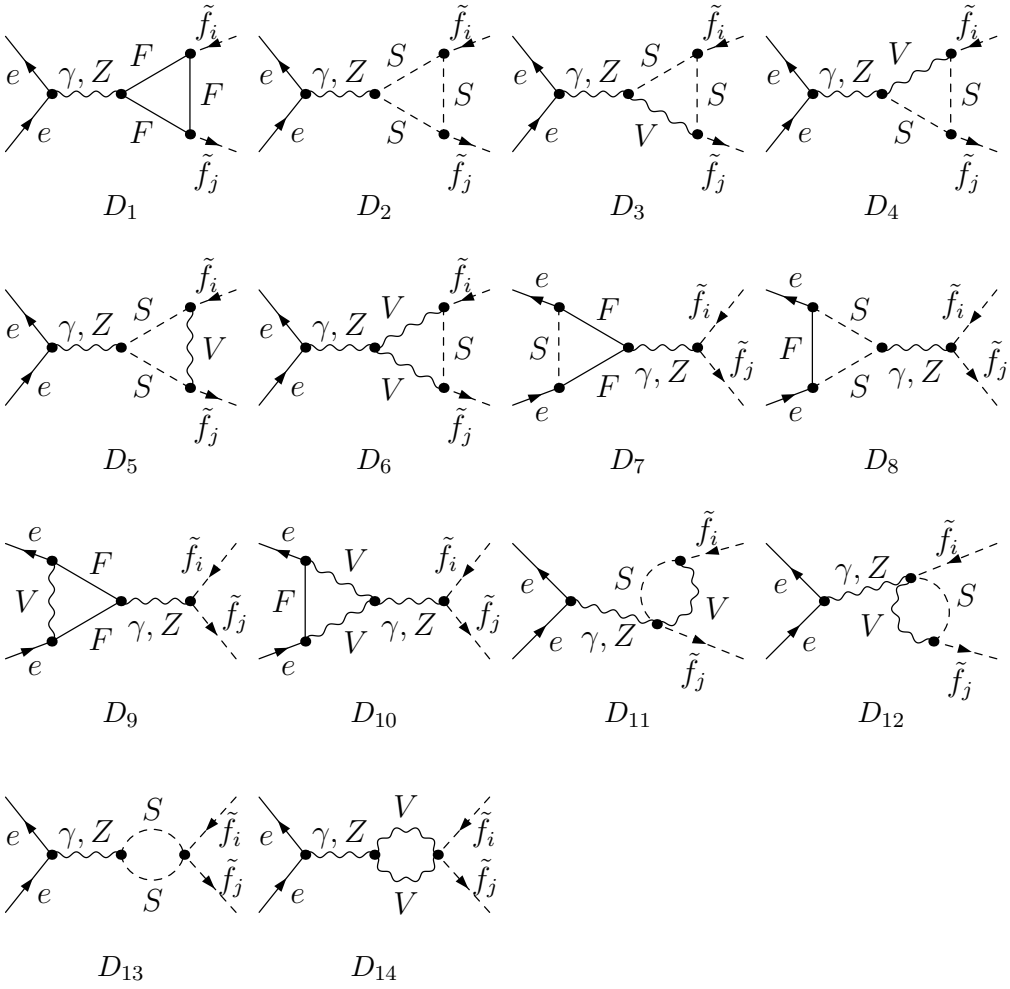

Figure 3: Vertex contributions to $e^+e^- \to \widetilde{f}_i\widetilde{f}_j^*$

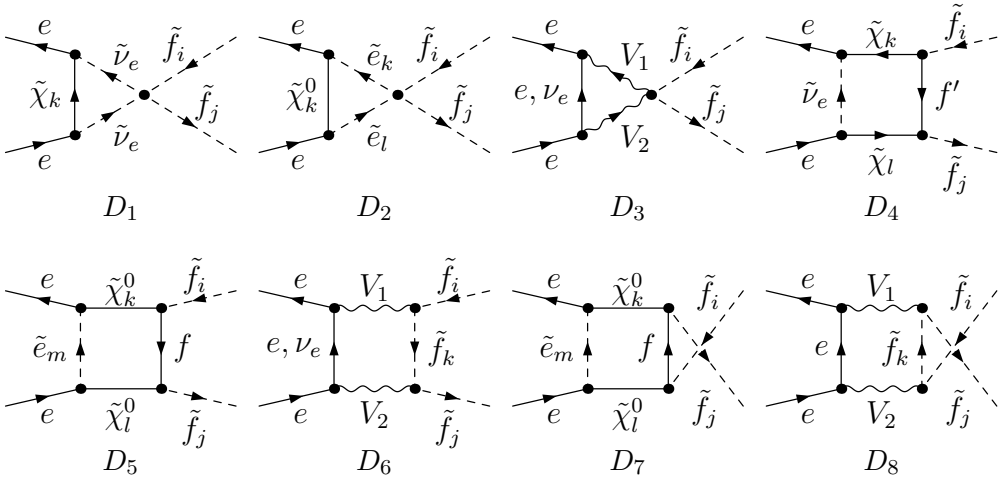

Figure 4: Boxes contributions to $e^+e^- \to \widetilde{f}_i\widetilde{f}_j^*$

3.2 Renormalization

During the last decade, several approaches for renormalization of the MSSM in the on-shell scheme have been developed [22] – [26] (see e.g. [27] for an overview). Here we follow the strategy of [22] by introducing counterterms for the physical parameters, i.e. for masses and mixing angles, and perform field renormalization in a way that residues of renormalized propagators can be kept at unity.

For the SM parameters and fields, we adopt the on-shell renormalization scheme in the specification of [28], with the following replacements for the parameters

$$e \to (1+\delta Z_e)e \qquad , \qquad M^2_{W,Z} \to M^2_{W,Z} + \delta M^2_{W,Z}\,, \tag{3.1}$$

and for the vector-boson fields

$$Z \to Z^{1/2}_{ZZ} Z + Z^{1/2}_{Z\gamma} A\,, \quad A \to Z^{1/2}_{AA} A + Z^{1/2}_{\gamma Z} Z\,, \quad \text{with} \quad Z^{1/2}_{ab} = \delta_{ab} + \frac{1}{2}\delta Z_{ab}\,. \tag{3.2}$$

By the on-shell definition of the electroweak mixing angle ($s_W = \sin\theta_W$, $c_W = \cos\theta_W$) according to $s^2_W = 1 - M^2_W/M^2_Z$, the corresponding counterterm is determined through the W and Z mass counterterms,

$$\frac{\delta s^2_W}{s^2_W} = \frac{c^2_W}{s^2_W}\left(\frac{\delta M^2_Z}{M^2_Z} - \frac{\delta M^2_W}{M^2_W}\right) \quad , \quad \frac{\delta c^2_W}{c^2_W} = \frac{\delta M^2_Z}{M^2_Z} - \frac{\delta M^2_W}{M^2_W}\,. \tag{3.3}$$

For the genuine SUSY part, we have to renormalize the scalar-fermion fields and the mixing angle $\widetilde{\theta}_f$ in (2.5), which is done by the substitution

$$\widetilde{f}_1 \to Z^{1/2}_{11}\widetilde{f}_1 + Z^{1/2}_{12}\widetilde{f}_2 \;\;,\;\; \widetilde{f}_2 \to Z^{1/2}_{22}\widetilde{f}_2 + Z^{1/2}_{21}\widetilde{f}_1 \;\;,\;\; \widetilde{\theta}_f \to \widetilde{\theta}_f + \delta\widetilde{\theta}_f \tag{3.4}$$

with $Z^{1/2}_{ij} = \delta_{ij} + \frac{1}{2}\delta Z_{ij}$.

Applying the prescriptions given above to the Lagrangian (2.8) yields the counterterm Lagrangian for the SUSY vertices in Fig. 5 as follows (the other counterms in Fig. 5 are formally the same as in the SM),

$$\delta\mathcal{L} \;=\; A^\mu \sum_{i,j=1,2} \delta(\gamma\widetilde{f}_i\widetilde{f}_j)\; \widetilde{f}^*_i \overleftrightarrow{\partial}_\mu \widetilde{f}_j + Z^\mu \sum_{i,j=1,2} \delta(Z\widetilde{f}_i\widetilde{f}_j)\; \widetilde{f}^*_i \overleftrightarrow{\partial}_\mu \widetilde{f}_j \tag{3.5}$$

where

$$\begin{aligned}
\delta(\gamma\widetilde{f}_i\widetilde{f}_j) &= -eQ_f(\frac{1}{2}\delta Z_{ij} + \frac{1}{2}\delta Z_{ji}) - eQ_f(\frac{1}{2}\delta Z_{\gamma\gamma} + \delta Z_e)\delta_{ij} + \frac{1}{2} g_{Z\widetilde{f}_i\widetilde{f}_j}\,\delta Z_{Z\gamma}\,, \\
\delta(Z\widetilde{f}_i\widetilde{f}_j) &= -eQ_f\frac{1}{2}\delta Z_{\gamma Z} + g_{Z\widetilde{f}_i\widetilde{f}_j}(\delta Z_e + \frac{1}{2}\delta Z_{ZZ}) \\
&\quad + \frac{\delta s_W e}{c^3_W s^2_W}[(-I^f_3 - Q_f s^2_W + 2I^f_3 s^2_W)R^{\widetilde{f}}_{j1}R^{\widetilde{f}}_{i1} - Q_f s^2_W R^{\widetilde{f}}_{j2}R^{\widetilde{f}}_{i2}] \\
&\quad + g_{Z\widetilde{f}_i\widetilde{f}_j}(\frac{1}{2}\delta Z_{ii} + \frac{1}{2}\delta Z_{jj}) + g_{Z\widetilde{f}_k\widetilde{f}_j}\delta Z_{ki} + g_{Z\widetilde{f}_i\widetilde{f}_l}\delta Z_{lj} + \Delta(g_{Z\widetilde{f}_i\widetilde{f}_j})\delta\widetilde{\theta}_f
\end{aligned} \tag{3.6}$$

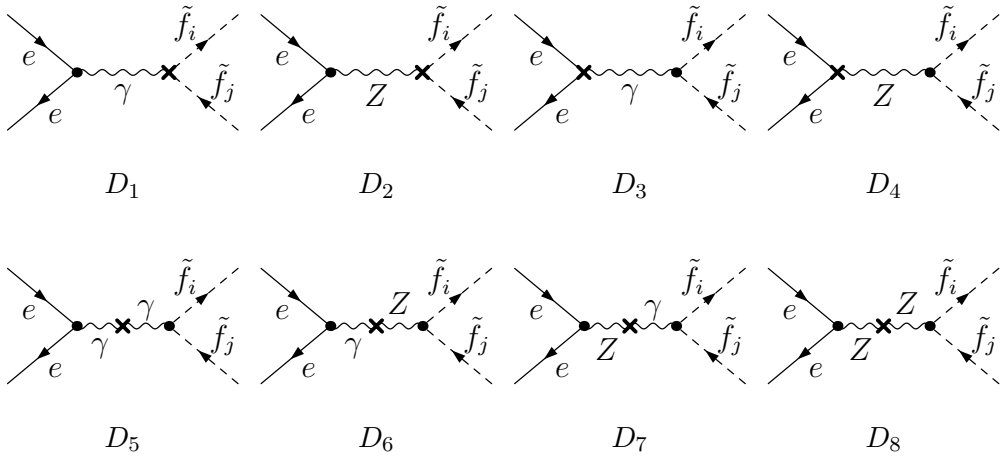

Figure 5: Counterterms for renormalizing the amplitudes for $e^+e^- \to \widetilde{f}_i \widetilde{f}_j^*$

with $\quad \Delta(g_{Z\widetilde{f}_1\widetilde{f}_1}) = -\Delta(g_{Z\widetilde{f}_2\widetilde{f}_2}) = 2g_{Z\widetilde{f}_1\widetilde{f}_2} \quad$ and $\quad \Delta(g_{Z\widetilde{f}_1\widetilde{f}_2}) = \Delta(g_{Z\widetilde{f}_2\widetilde{f}_1}) = g_{Z\widetilde{f}_2\widetilde{f}_2} - g_{Z\widetilde{f}_1\widetilde{f}_1}$.

To fix all the renormalization constants, the following conditions are imposed:

- The on-shell conditions for M_W, M_Z, m_f, e, and for the gauge-field renormalization constants as in the SM [28].
- On-shell conditions for the scalar fermions $\widetilde{f}_i$, specified by the requirements of mass renormalization, zero mixing on each mass shell, and residue =1 for the diagonal sfermion propagators,

$$\begin{aligned}
\delta Z_{11} &= \frac{\partial}{\partial p^2}\Sigma_{\widetilde{f}_1\widetilde{f}_1}(p^2)|_{p^2=m^2_{\widetilde{f}_1}} \quad , \quad \delta Z_{22} = \frac{\partial}{\partial p^2}\Sigma_{\widetilde{f}_2\widetilde{f}_2}(p^2)|_{p^2=m^2_{\widetilde{f}_2}} \, , \\
\delta Z_{12} &= \frac{\Sigma_{\widetilde{f}_1\widetilde{f}_2}(m^2_{\widetilde{f}_2})}{m^2_{\widetilde{f}_2} - m^2_{\widetilde{f}_1}} \, , \; \delta Z_{21} = \frac{\Sigma_{\widetilde{f}_2\widetilde{f}_1}(m^2_{\widetilde{f}_1})}{m^2_{\widetilde{f}_1} - m^2_{\widetilde{f}_2}} \quad , \quad \delta m^2_{\widetilde{f}_i} = \Sigma_{\widetilde{f}_i\widetilde{f}_j}(m^2_{\widetilde{f}_i}) \, , \\
\delta\widetilde{\theta}_f &= \frac{1}{2}\frac{\Sigma_{\widetilde{f}_1\widetilde{f}_2}(m^2_{\widetilde{f}_2}) + \Sigma_{\widetilde{f}_1\widetilde{f}_2}(m^2_{\widetilde{f}_1})}{m^2_{\widetilde{f}_2} - m^2_{\widetilde{f}_1}} \, ,
\end{aligned} \tag{3.7}$$

where $\sum_{\widetilde{f}_i\widetilde{f}_j}(p^2)$, $i,j = 1,2$ denotes the unrenormalized diagonal and non-diagonal sfermion self-energies. The condition for the sfermion mixing angle has also been used in [29] in the context of QCD corrections to squark decays. The sfermion-mass renormalization condition is listed for completeness; it is not needed for our actual computation.

3.3 Amplitudes and cross sections

In the limit of vanishing electron mass, the part of the amplitude following from the one-loop diagrams, $\mathcal{M}^1$, can be projected on the two invariants $I_{L,R}$ defined in eq. (2.10),

$$\mathcal{M}^1 = \mathcal{M}^1_L \; I_L + \mathcal{M}^1_R \; I_R \; + \cdots \tag{3.8}$$

The omitted terms are of the type $\bar{v}(1 \pm \gamma_5)u$; they vanish in the interference with $\mathcal{M}_0$ and are hence not required at one-loop order. For the counterterm part of the amplitude, $\delta\mathcal{M}^1$, the projection on these two invariants is exact,

$$\delta\mathcal{M}^1 = \delta\mathcal{M}^1_L \; I_L + \delta\mathcal{M}^1_R \; I_R \,. \tag{3.9}$$

The differential cross section can be written as follows,

$$\frac{d\sigma_1}{d\Omega} = \frac{d\sigma_0}{d\Omega} + \{ \; 2\,\Re[\mathcal{M}_0^*(\mathcal{M}^1 + \delta\mathcal{M}^1)] + |\mathcal{M}^1 + \delta\mathcal{M}^1|^2 \; \} \cdot \frac{1}{4} \, \frac{\kappa_{ij}}{64\pi^2 s} \tag{3.10}$$

(spin summation to be understood) with the Born cross section from (2.13). At one-loop order, only the interference term contributes,

$$\Re[\mathcal{M}_0^*(\mathcal{M}^1 + \delta\mathcal{M}^1)] = [\mathcal{M}^0_L(\mathcal{M}^1_L + \delta\mathcal{M}^1_L) + \mathcal{M}^0_R(\mathcal{M}^1_R + \delta\mathcal{M}^1_R)] \, \frac{s^2}{4}\kappa_{ij}^2 \sin^2\theta \,, \tag{3.11}$$

on which our numerical analysis is based. Nevertheless, we will comment also on the purely-quadratic term,

$$|\mathcal{M}^1 + \delta\mathcal{M}^1|^2 = (|\mathcal{M}^1_L + \delta\mathcal{M}^1_L|^2 + |\mathcal{M}^1_R + \delta\mathcal{M}^1_R|^2) \, \frac{s^2}{4}\kappa_{ij}^2 \sin^2\theta \,, \tag{3.12}$$

which may be useful to give some partial information on the size of higher-order corrections of $\mathcal{O}(\alpha^2)$.

The integrated cross section at the one-loop level, σ_1, derived from (3.10) with the interference term only, can be written in the following way,

$$\sigma_1 = \sigma_0 + \sigma_0 \Delta \,, \tag{3.13}$$

pointing out the relative correction

$$\Delta = (\sigma_1 - \sigma_0)/\sigma_0 \tag{3.14}$$

with respect to the Born cross section σ_0 in eq. (2.15).

The relative correction Δ can be decomposed into the following parts, indicating their origin,

$$\Delta = \Delta_{\text{self}} + \Delta_{\text{vertex}} + \Delta_{\text{boxes}} + \Delta_{\text{QED}} + \Delta_{\text{SUSY-QCD}} \tag{3.15}$$

where $\Delta_{\rm SUSY-QCD}$ denotes the supersymmetric QCD corrections with virtual gluinos as well as virtual and real gluons. The gluino part has been recalculated here in connection with the electroweak contributions, and the gluon part is taken over from [8].

The electroweak terms $\Delta_{\rm vertex}$ and $\Delta_{\rm boxes}$ do not contain any virtual-photon diagram. According to the discussion at the end of section 3.1, all virtual-photon diagrams for vertex, box, and external wave-function contributions have been properly separated and combined with real bremsstrahlung to form the subclass of QED corrections, described by $\Delta_{\rm QED}$.

We note that universal-type quantities, like self energies, initial and final state vertex corrections, do not generate any forward–backward asymmetry. Indeed, A_{FB} is only generated by non the universal part, essentially from box diagrams and real bremsstrahlung, as discussed later.

For the loop-induced forward–backward asymmetry A_{FB} we will apply the same definition as in [21],

$$A_{FB} = \frac{\sigma_F - \sigma_B}{\sigma} = \frac{\sigma_F - \sigma_B}{\sigma_0}\frac{1}{1+\Delta} = \Delta_{FB}\frac{1}{1+\Delta}\,. \tag{3.16}$$

Δ_{FB} is the antisymmetric part of the cross section normalized to the Born cross section σ_0.

4 Numerical evaluation and discussion

To set the basis for the numerical evaluation, we specify the free parameters that will be used.

- The MSSM Higgs sector is parametrized by the CP-odd mass M_A and $\tan\beta$, taking into account radiative corrections with the help of FeynHiggs [30], and we assume $\tan\beta \geq 2.5$.
- The chargino–neutralino sector can be parametrized by the gaugino-mass terms M_1, M_2, and the Higgsino-mass term μ. For simplification we assume $M_1 \approx M_2/2$.
- Sfermions are characterized by a common soft-breaking sfermion mass $M_{SUSY} \equiv \widetilde{M}_L = \widetilde{M}_R$ and soft trilinear couplings A_f. Again, for simplicity, we will take them as uniform for $\tilde{t}$, $\tilde{b}$, and τ ($A_0 \equiv A_t = A_b = A_\tau$).

As experimental data points [31], the following input quantities enter: $\alpha^{-1} = 137.03598$, $m_Z = 91.1875$ GeV, $m_W = 80.45$ GeV, $m_t = 174.3$ GeV.

Before presenting our results, we want to mention that we performed cross checks with the results of [15] for the subclass of Yukawa corrections considered there and found perfect agreement for $\tilde{t}$ and $\tilde{b}$ production [2]. Furthermore, QED corrections, self energies, boxes, and SUSY-QCD corrections have been checked with independent calculations not based on FormCalc.

For illustration of the effects of the radiative corrections, we have chosen the following three scenarios:

[2] For $\tilde{b}$ production we got agreement after correcting an overall sign in the charged Higgs contribution in [15].

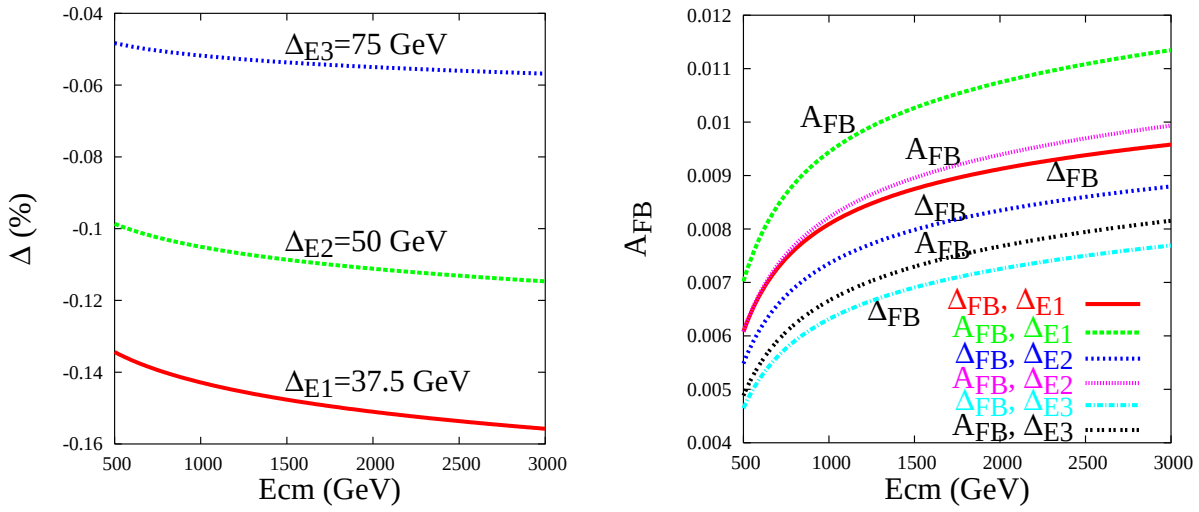

Figure 6: QED corrections to the total cross section (left) and the forward-backward asymmetry (right) for $e^+e^- \to \widetilde{b}_1\widetilde{b}_1^*$ in scenario sc_1, as function of the CM energy $E_{\rm CM} = \sqrt{s}$.

sc_1: $\tan\beta = 6$, $M_A = 250$, $M_{SUSY} = 200$, $\mu = 800$, $M_2 = 200$ and $A_0 = 400$ GeV.
$m_{\widetilde{\tau}_{1,2}} = (185, 223)$ GeV, $m_{\widetilde{t}_{1,2}} = (148, 339)$ GeV, $m_{\widetilde{b}_{1,2}} = (146, 250)$ GeV,
$m_{\widetilde{c}_{1,2}} = m_{\widetilde{c}_{L,R}} = (193, 197)$ GeV, $m_{\widetilde{s}_{1,2}} = m_{\widetilde{s}_{R,L}} = (201, 209)$ GeV; $m_{\tilde{g}} = 525$ GeV.

sc_2: $\tan\beta = 18$, $M_A = 250$, $M_{SUSY} = 400$, $\mu = 1600$, $M_2 = 200$ and $A_0 = 800$ GeV.
$m_{\widetilde{\tau}_{1,2}} = (335, 460)$ GeV, $m_{\widetilde{t}_{1,2}} = (254, 559)$ GeV, $m_{\widetilde{b}_{1,2}} = (175, 542)$ GeV,
$m_{\widetilde{c}_{1,2}} = m_{\widetilde{c}_{L,R}} = (396, 399)$ GeV, $m_{\widetilde{s}_{1,2}} = m_{\widetilde{s}_{R,L}} = (397, 408)$ GeV; $m_{\tilde{g}} = 524$ GeV.

sc_3: $\tan\beta = 30$, $M_A = 250$, $M_{SUSY} = 200$, $\mu = 200$, $M_2 = 1000$ and $A_0 = 300$ GeV.
$m_{\widetilde{\tau}_{1,2}} = (179, 228)$ GeV, $m_{\widetilde{t}_{1,2}} = (131, 346)$ GeV, $m_{\widetilde{b}_{1,2}} = (124, 263)$ GeV,
$m_{\widetilde{c}_{1,2}} = m_{\widetilde{c}_{L,R}} = (192, 197)$ GeV, $m_{\widetilde{s}_{1,2}} = m_{\widetilde{s}_{R,L}} = (201, 209)$ GeV; $m_{\tilde{g}} = 2624$ GeV.

sc_1 is gaugino-like with rather light sfermions, and sc_2 is also gaugino-like with intermediate $\tan\beta$, and heavier sfermions, and sc_3 is higgsino-like with large $\tan\beta = 30$.

As explained before, QED corrections can be isolated and can be studied separately. The corrections depend on the values of the photon-energy cut ΔE. More realistic situations require more complicated cuts and a more sophisticated treatment of the real photon part. Nevertheless, we display $\Delta_{\rm QED}$ in Fig. 6 to indicate the size of the QED effects, for various energy cuts. Fig. 6 is for scenario sc_1 and for the special case of $\tilde{b}_1$-pair production. The behavior for other scenarios and fermion states is almost the same, as long as one is away from the thresholds localized at different energies, where the Coulomb singularity shows up. Also given in Fig. 6 is the QED-induced forward-backward asymmetry, which is very small, well below 1% up to the TeV range. In the case of QED corrections, large double-logarithms of the Sudakov type are absent due to cancellations by the bremsstrahlung contributions.

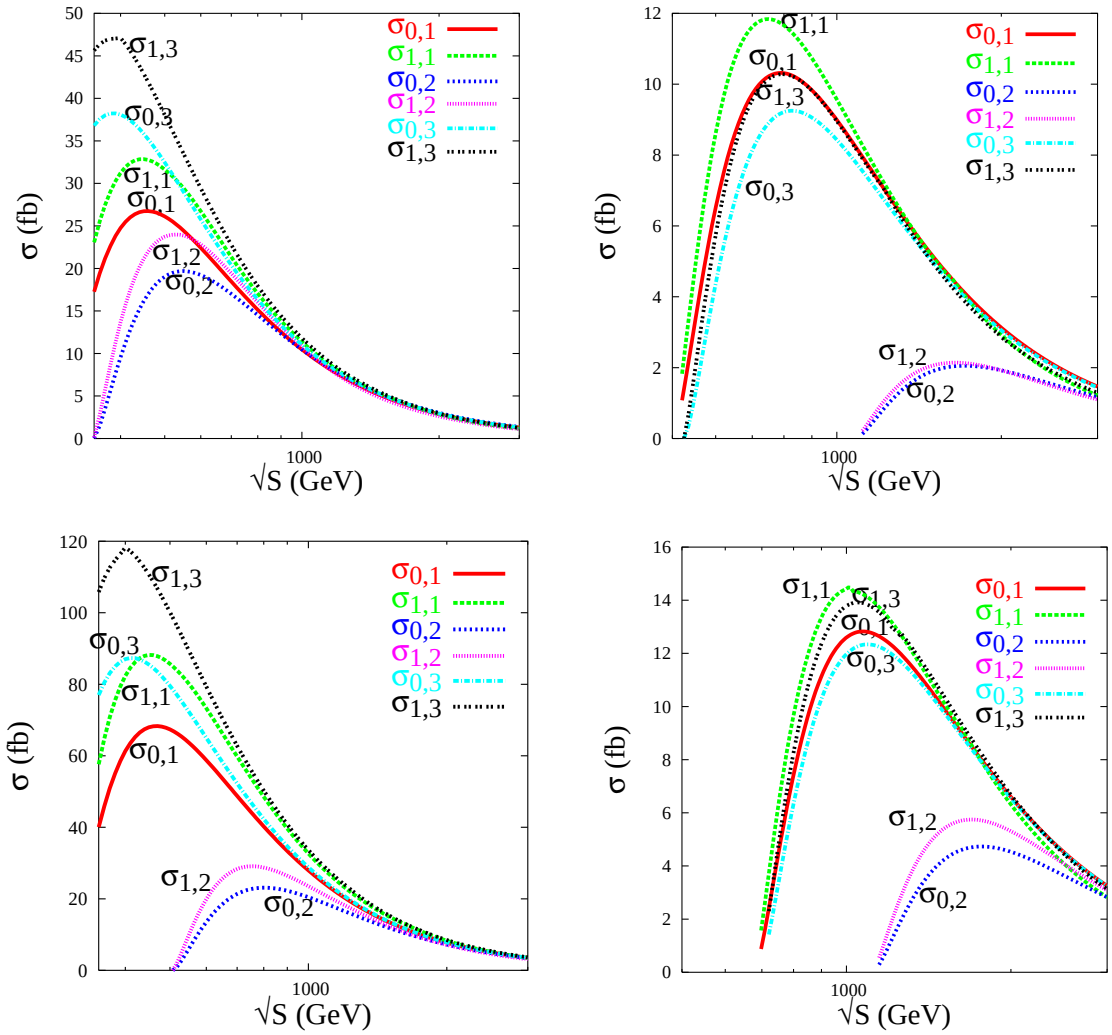

Figure 7: Integrated tree-level cross sections $\sigma_{0,i}$ and one-loop cross section $\sigma_{1,i}$ in the three scenarios ($i = sc_1, sc_2, sc_3$) for $e^+e^- \to \tilde{b}_k\tilde{b}_k^*$ (upper part) and $e^+e^- \to \tilde{t}_k\tilde{t}_k^*$ (lower part). The lighter squarks ($k = 1$) are on the left, the heavier squarks ($k = 2$) on the right side.

Our main emphasis will be on the residual set of non-QED corrections, which involve the quantum structure of the complete MSSM. In all the figures of the following discussions, the QED corrections are not included.

Third-generation squarks

In Fig. 7 we show the integrated tree-level cross section $\sigma_{0,i}$ for our three scenarios ($i = sc_1, sc_2, sc_3$) and the corresponding one-loop cross section $\sigma_{1,i}$ for the squarks of the third generation ($\tilde{q} = \tilde{b}, \tilde{t}$), $e^+e^- \to \tilde{q}_1\tilde{q}_1^*$ and $e^+e^- \to \tilde{q}_2\tilde{q}_2^*$, as function of the center of mass energy. As it can be seen in Fig. 7, in the energy range where the cross sections are large, the loop contributions lead to a further significant enhancement.

In order to outline the loop contributions more directly, we display in Fig. 8 ($\tilde{b}$ squarks) and Fig. 9 ($\tilde{t}$ squarks) the relative corrections to the cross sections and show also the

$\sqrt{s}$	500GeV		1.5 TeV		3 TeV	
sc_1	-.074	-.073	-.22	-.20	-.36	-.32
sc_2	-.049	-.048	-.17	-.16	-.31	-.28

Table 1: Relative corrections from the interference term (left column) and with the quadratic one-loop term (right column) of eq. (3.10)

breakdown into their various subclasses.

A substantial fraction is due to the SUSY-QCD corrections, which in general are dominated by the conventional real- and virtual-gluon contributions. One can see in Figs. 8, 9 the enhancement for $\sqrt{s} \to 2m_{\widetilde{f}_i}$, which indicates the QCD equivalent of the QED Coulomb singularity, studied in [14, 7] for slepton-pair production. The gluon contributions are always positive and sizeable, and the gluino contributions are usually small. Only at very high energies the gluino effects can become more important; they are negative and diminish the gluon-QCD corrections. In scenario 2, for example, at $\sqrt{s} = 3$ TeV, the gluino correction can reach about -8% for $\widetilde{b}_1\widetilde{b}_1^*$, -13% for $\widetilde{b}_2\widetilde{b}_2^*$, -7% for $\widetilde{t}_1\widetilde{t}_1^*$, and -18% for $\widetilde{t}_2\widetilde{t}_2^*$ final states.

At very high energies $\sqrt{s} \gg M_W$, large single and double logarithms of the ratio s/M_W^2 become dominating. Self energies contain only single logarithms, which correspond to the evolution of running coupling constants. Box diagrams contain Sudakov logarithms of the type $\log^2(s/M^2)$ (where M is a generic mass of internal particles), which are large and negative. The dominant contributions arise from diagrams with the exchange of standard gauge bosons. The leading effect at high energies thus comes from the box diagrams and can reach up to -40% (-25%) in case of bottom squarks (top squarks). From Figs. 8, 9 one can see that the large box effects interfere destructively with SUSY-QCD and self-energy corrections, yielding e.g. a total relative correction of about -20% in scenario 2 (1) for $e^+e^- \to \widetilde{b}_{1(2)}\widetilde{b}_{1(2)}^*$.

For very high energies, higher-order corrections have to be considered as well. Without entering a two-loop computation, one get at least some partial information on the size of the $\mathcal{O}(\alpha^2)$ corrections from the square of the one-loop amplitude in (3.10). As an example, we will give in the Table 1 for the case of $e^+e^- \to \widetilde{b}_1\widetilde{b}_1^*$ some numerical values to illustrate the effect from the square of the one-loop amplitude, of $\mathcal{O}(\alpha^2)$. Only the dominating box contributions, with gauge-boson exchanges ($D_{6,8}$ with $V_{1,2} = Z, W$) are shown. The first column is the interference term of $\mathcal{O}(\alpha)$ [eq. (3.11)] and the second column includes also the one-loop square term [eq. (3.12)] of $\mathcal{O}(\alpha^2)$/ As one can see, at lower energies $\sqrt{s} < 1$ TeV, the effect is marginal (around 1%), while at high energy the cross section can be reduced by several per cent.

In refs. [11, 12] general one-loop expressions of the leading quadratic and subleading linear logarithms of Sudakov type and also the corresponding resummation to subleading logarithms are derived. It is difficult to do a quantitative comparison because the input is

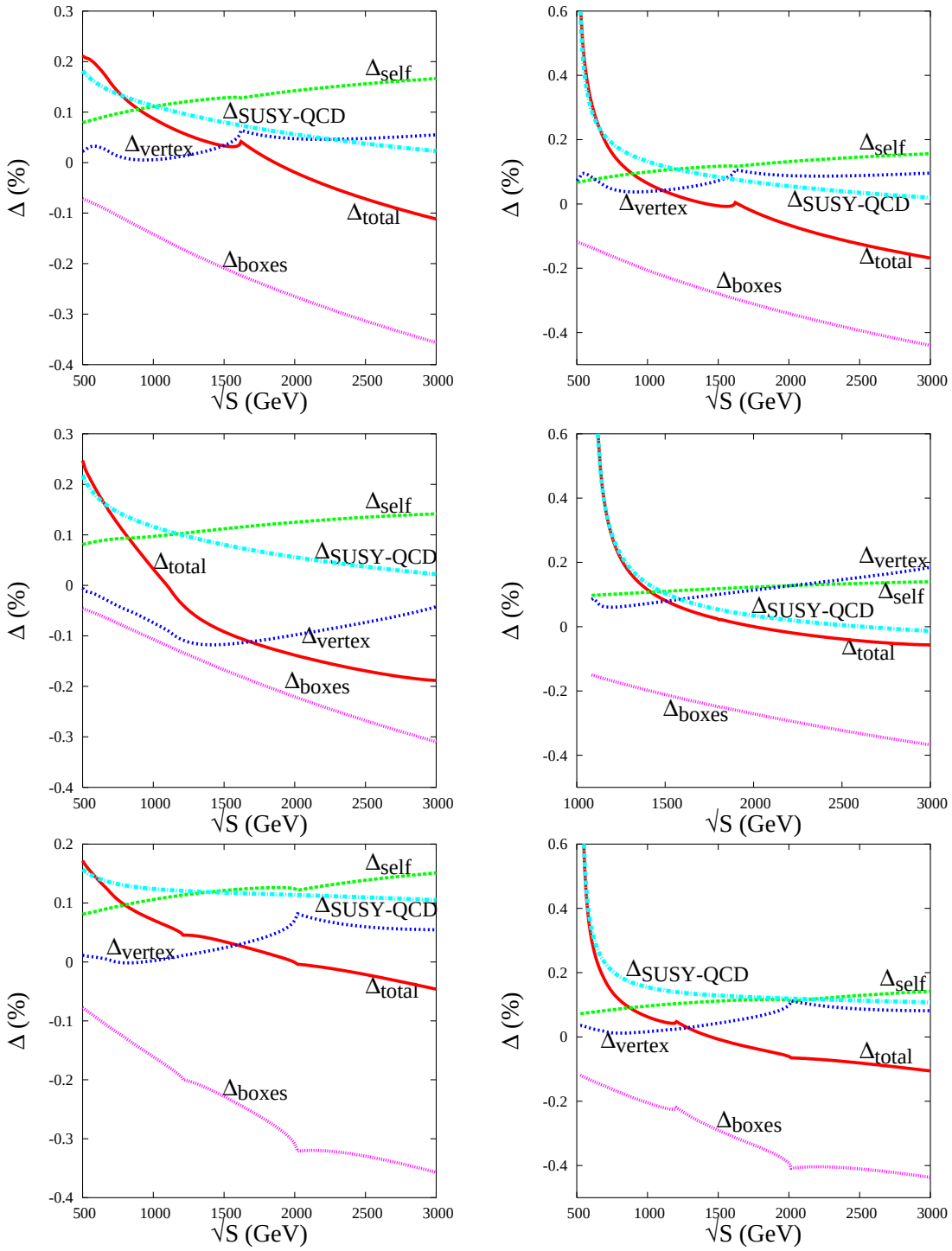

Figure 8: Electroweak and SUSY-QCD corrections to $e^+e^- \to \tilde{b}_1\tilde{b}_1^*$ (left) and $e^+e^- \to \tilde{b}_2\tilde{b}_2^*$ (right). Scenario sc_1 (upper plots), sc_2 (middle plots), and sc_3 (lower plots).

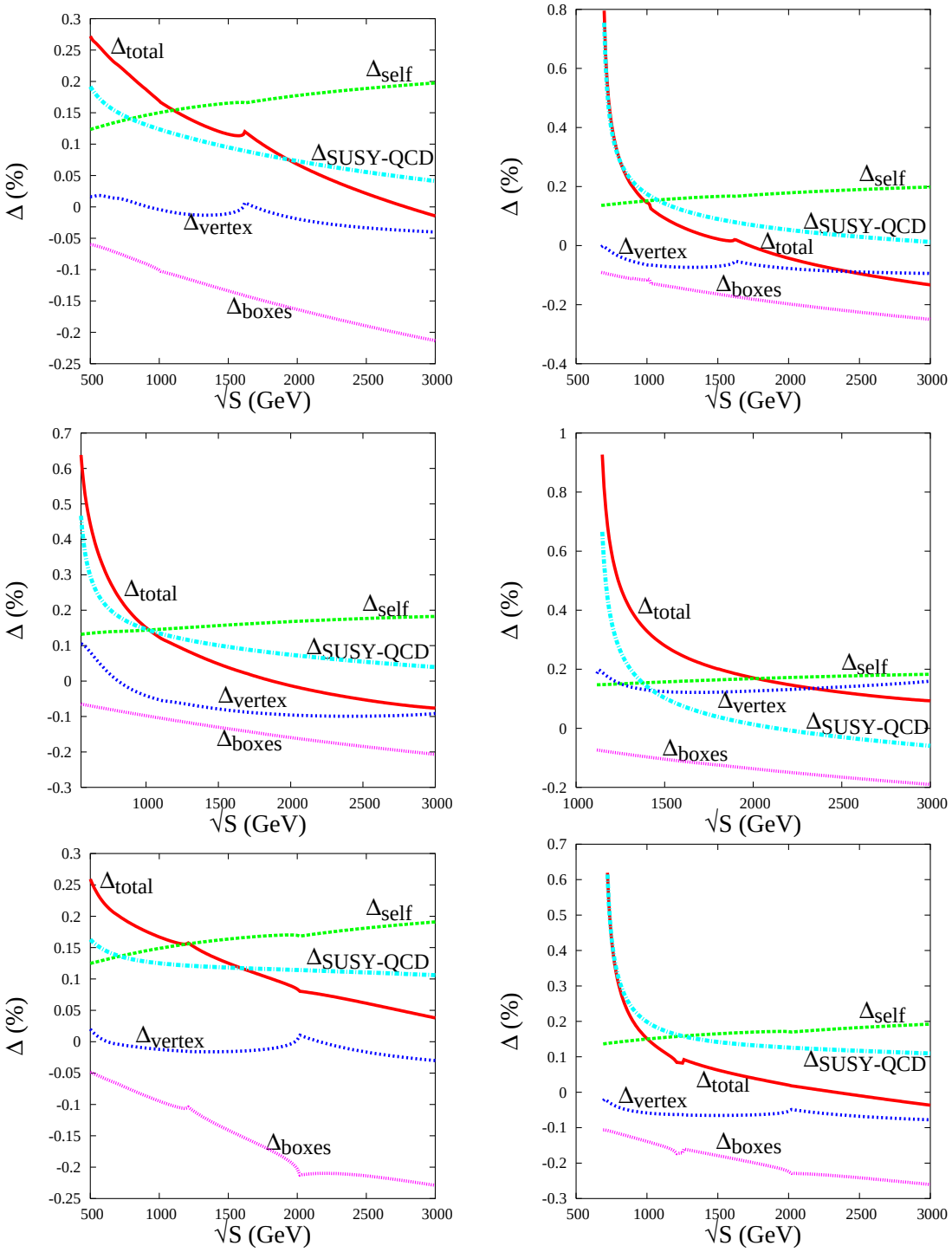

Figure 9: Electroweak and SUSY-QCD corrections to $e^+e^- \to \tilde{t}_1\tilde{t}_1^*$ (left) and $e^+e^- \to \tilde{t}_2\tilde{t}_2^*$ (right). Scenario sc_1 (upper plots), sc_2 (middle plots), and sc_3 (lower plots).

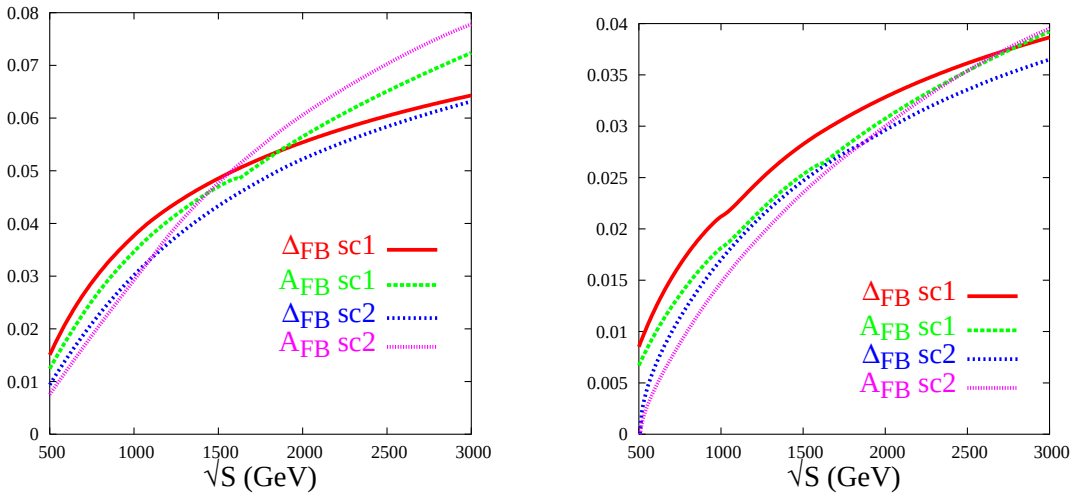

Figure 10: Forward-backward asymmetry for $e^+e^- \to \tilde{b}_1\tilde{b}_1^*$ (left) and $e^+e^- \to \tilde{t}_1\tilde{t}_1^*$ (right) as function of center of mass energy for scenarios $sc_{1,2}$

not completely specified in [11, 12], but the results are in qualitative agreement with ours.

We want to illustrate also the loop-induced forward-backward asymmetry, selecting sc_1 and sc_2 as examples in Fig. 10. Contrary to the QED case, where only photon and Z are exchanged in box graphs, the presence of neutralinos, charginos, and heavy gauge bosons in the box diagrams generates forward-backward asymmetries of several per cent, about 4% (7%) at 1.5 TeV (3 TeV) for $e^+e^- \to \tilde{b}_1\tilde{b}_1^*$. In the case of $e^+e^- \to \tilde{t}_1\tilde{t}_1^*$, the asymmetry is smaller by a factor 1/2.

Finally, we examine the production of a non-diagonal squark pair $\tilde{f}_1\tilde{f}_2^*$. Because of electromagnetic invariance, the photon does not couple to a pair of $\tilde{f}_1$ $\tilde{f}_2^*$. Consequently, at tree level, the reaction $e^+e^- \to \tilde{f}_1\tilde{f}_2^*$ proceeds only through s-channel Z-boson exchange. The cross section for $e^+e^- \to \tilde{f}_1\tilde{f}_2^*$ is thus directly determined by the $Z\tilde{f}_1\tilde{f}_2^*$ coupling, which is proportional to $\sin 2\tilde{\theta}_f$ of the sfermion-mixing angle $\tilde{\theta}_f$. The measurement of such a process can determine efficiently the value of the mixing angle and also the mass of $\tilde{f}_2$ [4]. This is complementary to other methods proposed to measure the mixing angle, which are based on $e^+e^- \to \tilde{t}_1\tilde{t}_1^*$ with polarized beams [4, 32]. As shown in Fig. 11 for scenarios sc_1 and sc_3, the cross sections for $e^+e^- \to \tilde{t}_1\tilde{t}_2^*$ and $e^+e^- \to \tilde{b}_1\tilde{b}_2^*$ reach several femtobarn, which can lead to hundreds of events for a linear collider with 500 fb^{-1} integrated luminosity [4].

Without going into details, we mention that the self-energy contributions are smaller than in the case of diagonal $\tilde{f}_i\tilde{f}_i^*$ production, and vertex corrections are more sizeable. Box contributions are of about the same size as in the diagonal case for $\tilde{b}_1\tilde{b}_2^*$, and are by a factor 2 bigger for $\tilde{t}_1\tilde{t}_2^*$ compared to $\tilde{t}_i\tilde{t}_i^*$.

Fig. 11 contains also the SUSY-QCD corrections. One can see that at lower energies $\sqrt{s} \leq 1$ TeV, the corrections are dominated by the SUSY-QCD terms. At higher energies above 1

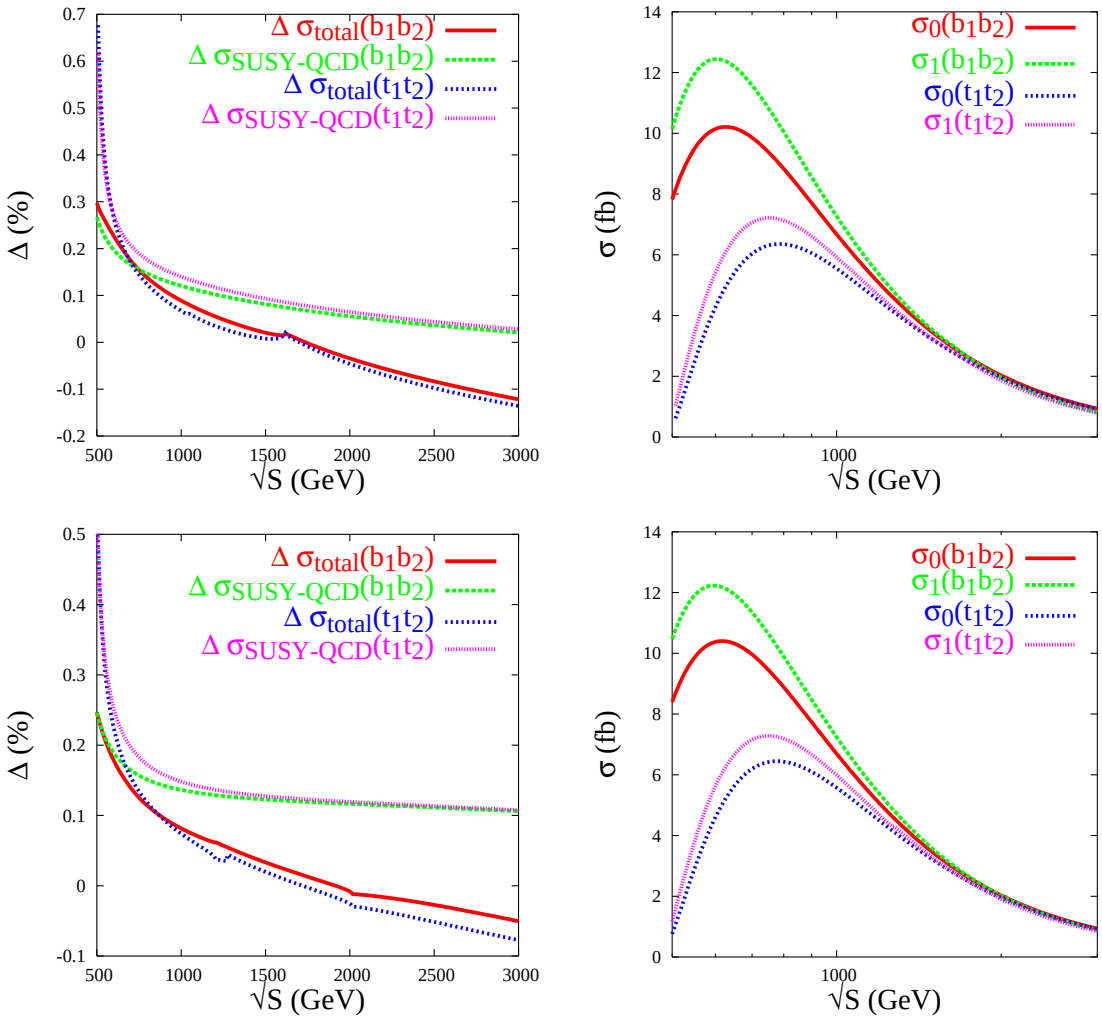

Figure 11: SUSY-QCD and total correction (left) and tree-level and one-loop cross section (right) for $e^+e^- \to (\widetilde{t}_1\widetilde{t}_2^*, \widetilde{b}_1\widetilde{b}_2^*)$. Scenario sc_1 (upper plots) and sc_3 (lower plots)

TeV, the box contributions turn out to be sizeable again and even dominate, driving the correction negative. We note that the forward-backward asymmetry for the off-diagonal pair production $e^+e^- \to \widetilde{f}_1\widetilde{f}_2^*$, also loop-induced, is of the same order as for $e^+e^- \to \widetilde{b}_1\widetilde{b}_1^*$.

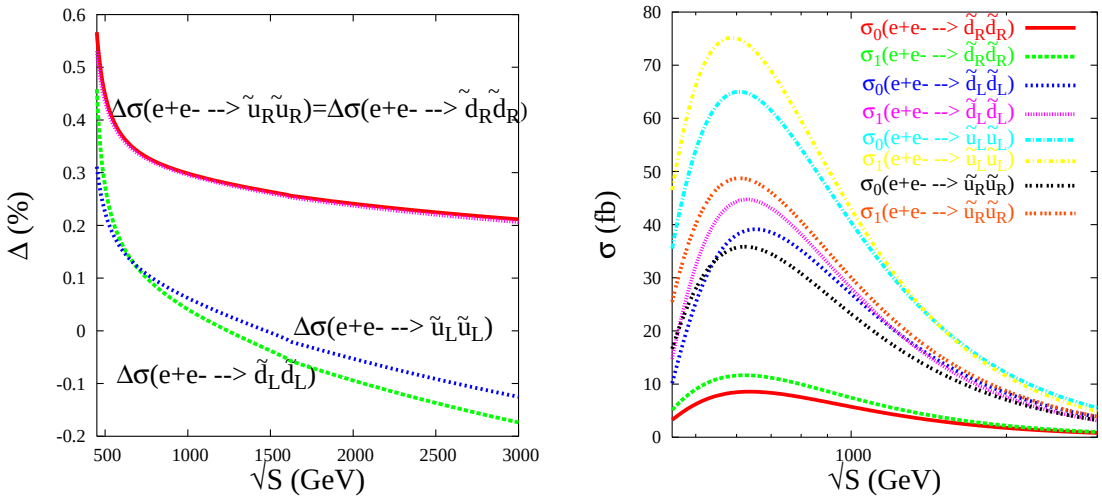

Figure 12: Total relative correction to first- and second-generation (up and down) squarks (left) and tree-level and one-loop cross sections (right), for scenarios $sc_{1,3}$

First- and second-generation squarks

We address now the production of squarks of the first and second generation. Since the corresponding quark masses are small, the squark-mixing angles practically vanish, according to eq. (2.7). For our scenarios with common $\widetilde{M}_L = \widetilde{M}_R$, we have $\widetilde{d}_{1,2} = \widetilde{d}_{R,L}$ and $\widetilde{u}_{1,2} = \widetilde{u}_{L,R}$. As an example, in sc_1, we display in Fig. 12 the tree-level and one-loop cross sections together with the relative correction for $e^+e^- \to \widetilde{q}_i\widetilde{q}_i$, $q = u, d$. The relative corrections $\Delta(e^+e^- \to \widetilde{q}_L\widetilde{q}_L)$ and $\Delta(e^+e^- \to \widetilde{q}_R\widetilde{q}_R)$ have almost the same shape for up and down squarks. The relative corrections $\Delta(e^+e^- \to \widetilde{q}_L\widetilde{q}_L)$ for the left-handed squarks are negative at high energies, while $\Delta(e^+e^- \to \widetilde{q}_R\widetilde{q}_R)$ for the right-handed squarks are positive. This behavior is due to the fact that for right-handed squarks QCD corrections dominate and thus remain positive even at high energy, while for left-handed squarks box diagrams are dominant being large and negative at high energy. We recall that i) the box contribution is dominated by the exchange of W and Z bosons, diagrams $D_{6,8}$ of Fig. 4, ii) the right-handed squarks do not couple to W bosons and thus the box contribution is small (compared to QCD corrections), even at high energy.

τ sleptons

In the case of $\widetilde{\tau}$-pair production, $e^+e^- \to \widetilde{\tau}_i\widetilde{\tau}_j^*$, shown in Fig. 13, the situation is different. There are no QCD corrections, and the vertex corrections are rather small, of the order of $\pm 2\%$. The dominant contribution is coming from self energies and boxes. The self-energy contributions are positive in the three scenarios, while the box contribution is always negative. This leads to a destructive interference between boxes and self energies, keeping the overall corrections comparatively small. At very high energies, the self-energy corrections (which get to the order of 20%) are reduced by box and vertex corrections to a net effect resulting in less than 10 %. As illustrated in Fig. 13, the radiative corrections to $e^+e^- \to \widetilde{\tau}_2\widetilde{\tau}_2^*$ have almost the same order of magnitude as $e^+e^- \to \widetilde{\tau}_1\widetilde{\tau}_1^*$ and are positive, while the corrections to $e^+e^- \to \widetilde{\tau}_1\widetilde{\tau}_2^*$ turn out to be negative. This is due to the fact that

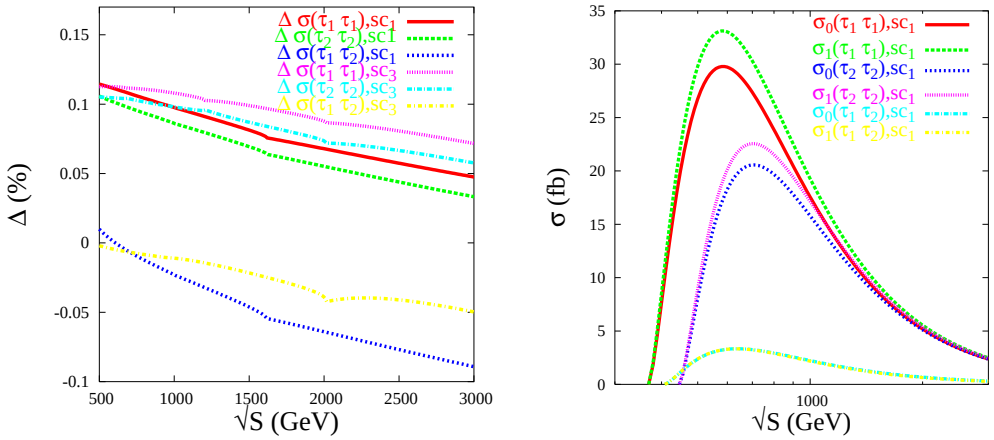

Figure 13: Total relative correction to $e^+e^- \to \widetilde{\tau}_i\widetilde{\tau}_j^*$ (scenarios sc_1 and sc_2, left) and tree-level and one-loop cross sections (scenario sc_1, right) as functions of the CM energy

box corrections to $e^+e^- \to \widetilde{\tau}_1\widetilde{\tau}_2^*$ are the dominant ones.

5 Conclusion

We have performed a full one-loop calculation of scalar-fermion pair production in e^+e^- annihilation in the on-shell scheme, comprising electroweak and SUSY-QCD contributions. We have studied the radiative corrections to third-generation scalar fermions $\widetilde{t}, \widetilde{b}, \widetilde{\tau}$ as well as to the first and second generation of scalar quarks. The QED contributions can be isolated, as a separate subclass, and the remaining set of one-loop corrections can be written as the sum of SUSY-QCD, self-energies, vertex corrections, and box contributions. It has been shown that the self-energy and QCD corrections always interfere destructively with the box diagrams. At low center-of-mass energies, the corrections are dominated by QCD, while at high energy the box contributions dominate. Box diagrams also induce forward-backward asymmetries of several per cent. We have evaluated the radiative corrections to both diagonal and off-diagonal pair production; processes like $e^+e^- \to \widetilde{f}_1\widetilde{f}_2^*$ may be useful to extract the mixing angles of the third generation. In general, the size of the loop effects, typically of the order 10 – 20 %, makes their proper inclusion in phenomenological studies and analyses for future e^+e^- colliders indispensable.

Acknowledgment:

A. Arhrib acknowledges the Alexander von Humboldt Foundation. Part of this work was done within the framework of the Associate Scheme of ICTP. A. A. thanks ICTP for the warm hospitality extended to him. We are grateful Thomas Hahn for computing assistance and useful discussions, as well as to T. Fritzsche and H. Rzehak. We also want to thank H. Eberl for helpful communications.

References

[1] H.E. Haber and G.L. Kane, Phys. Rep. 117 (1985) 75; H.P. Nilles, Phys. Rep. 110 (1984) 1; P. Nath, R. Arnowitt and A. Chamseddine, "Applied N=1 Supergravity", ITCP Series in Theoretical Physics, World Scientific, Singapore 1984;
X.R. Tata, in Proceedings of the "Mt Sorak Symposium on the Standard Model and Beyond", Mt Sorak, Korea, 1990

[2] T. Affolder *et al.* [CDF Collaboration], Phys. Rev. D **63**, 091101 (2001); [arXiv:hep-ex/0011004]. F. Abe *et al.* [CDF Collaboration], Phys. Rev. D **56**, 1357 (1997); B. Abbott *et al.* [D0 Collaboration], Phys. Rev. Lett. **83**, 4937 (1999) [arXiv:hep-ex/9902013].

[3] G. Abbiendi *et al.* [OPAL Collaboration], Phys. Lett. B **545**, 272 (2002) [Erratum-ibid. B **548**, 258 (2002)] [arXiv:hep-ex/0209026]; P. Abreu *et al.* [DELPHI Collaboration], Phys. Lett. B **496**, 59 (2000) [arXiv:hep-ex/0103034]; M. Acciarri *et al.* [L3 Collaboration], Phys. Lett. B **471**, 308 (1999) [arXiv:hep-ex/9910020].

[4] TESLA Technical Design Report, DESY 2001-011; J. A. Aguilar-Saavedra *et al.* [ECFA/DESY LC Physics Working Group Collaboration], arXiv:hep-ph/0106315; K. Abe *et al.* [ACFA Linear Collider Working Group Collaboration], arXiv:hep-ph/0109166; T. Abe *et al.* [American Linear Collider Working Group Collaboration], in *Proceedings of the APS/DPF/DPB Summer Study on the Future of Particle Physics (Snowmass 2001)* ed. N. Graf, arXiv:hep-ex/0106056.

[5] W. Beenakker, R. Höpker, M. Spira and P. M. Zerwas, Nucl. Phys. B **492**, 51 (1997) [arXiv:hep-ph/9610490]; W. Beenakker, R. Höpker, M. Spira and P. M. Zerwas, Phys. Rev. Lett. **74**, 2905 (1995) [arXiv:hep-ph/9412272].

[6] J. L. Feng and D. E. Finnell, Phys. Rev. D **49**, 2369 (1994) [arXiv:hep-ph/9310211]; T. Tsukamoto, K. Fujii, H. Murayama, M. Yamaguchi and Y. Okada, Phys. Rev. D **51**, 3153 (1995); A. Bartl, H. Eberl, S. Kraml, W. Majerotto, W. Porod and A. Sopczak, Z. Phys. C **76**, 549 (1997) [arXiv:hep-ph/9701336]; R. Keranen, A. Sopczak, H. Nowak and M. Berggren, Eur. Phys. J. directC **2** (2000) 7; R. Kitano, T. Moroi and S. F. Su, JHEP **0212**, 011 (2002) [arXiv:hep-ph/0208149]; E. L. Berger, J. Lee and T. M. Tait, arXiv:hep-ph/0306110.

[7] M. Drees and K. I. Hikasa, Phys. Lett. B **252**, 127 (1990).

[8] A. Arhrib, M. Capdequi-Peyranere and A. Djouadi, Phys. Rev. D **52**, 1404 (1995) [arXiv:hep-ph/9412382].

[9] H. Eberl, A. Bartl and W. Majerotto, Nucl. Phys. B **472**, 481 (1996) [arXiv:hep-ph/9603206].

[10] W. Beenakker, R. Höpker and P. M. Zerwas, Phys. Lett. B **349**, 463 (1995) [arXiv:hep-ph/9501292]; K. I. Hikasa and J. Hisano, Phys. Rev. D **54**, 1908 (1996) [arXiv:hep-ph/9603203].

[11] M. Beccaria, M. Melles, F. M. Renard and C. Verzegnassi, Phys. Rev. D **65**, 093007 (2002) [arXiv:hep-ph/0112273] and [arXiv:hep-ph/0210283].

[12] M. Beccaria, M. Melles, F. M. Renard, S. Trimarchi and C. Verzegnassi, [arXiv:hep-ph/0304110].

[13] A. Freitas *et al.*, [arXiv:hep-ph/0211108].

[14] A. Freitas, D. J. Miller and P. M. Zerwas, Eur. Phys. J. C **21**, 361 (2001) [arXiv:hep-ph/0106198].

[15] H. Eberl, S. Kraml and W. Majerotto, JHEP **9905**, 016 (1999) [arXiv:hep-ph/9903413].

[16] J. F. Gunion, H. E. Haber, G. L. Kane and S. Dawson, SCIPP-89/13, (Addison–Wesley, Reading, 1990).

[17] J. Küblbeck, M. Böhm, A. Denner, Comput. Phys. Commun. **60**, 165 (1990); T. Hahn, Comput. Phys. Commun. **140**, 418 (2001); T. Hahn, C. Schappacher, Comput. Phys. Commun. **143**, 54 (2002); T. Hahn, M. Perez-Victoria, Comput. Phys. Commun. **118**, 153 (1999);

[18] G. J. van Oldenborgh, Comput. Phys. Commun. **66**, 1 (1991); T. Hahn, Acta Phys. Polon. B **30**, 3469 (1999)

[19] W. Siegel, Phys. Lett. B **84**, 193 (1979). D. M. Capper, D. R. Jones and P. van Nieuwenhuizen, Nucl. Phys. B **167**, 479 (1980).

[20] A. Arhrib and G. Moultaka, Nucl. Phys. B **558**, 3 (1999) [arXiv:hep-ph/9808317].

[21] J. Guasch, W. Hollik and A. Kraft, Nucl. Phys. B **596** (2001) 66.

[22] J. Guasch, W. Hollik and J. Sola, JHEP **0210**, 040 (2002) [arXiv:hep-ph/0207364]. Phys. Lett. B **437**, 88 (1998) [arXiv:hep-ph/9802329].

[23] T. Fritzsche and W. Hollik, Eur. Phys. J. C **24**, 619 (2002) [arXiv:hep-ph/0203159].

[24] W. Öller, H. Eberl, W. Majerotto and C. Weber, Eur. Phys. J. C **29**, 563 (2003). [arXiv:hep-ph0304006]

[25] W. Hollik and H. Rzehak, [arXiv:hep-ph/0305328], to appear in Eur. Phys. J. C.

[26] W. Hollik, E. Kraus, M. Roth, C. Rupp, K. Sibold and D. Stöckinger, Nucl. Phys. B **639**, 3 (2002) [arXiv:hep-ph/0204350].

[27] W. Majerotto, [arXiv:hep-ph/0209137], Proceedings of the 10th International Conference on *Supersymmetry and Unifications of Fundamental Interactions (SUSY 02)*, eds. P. Nath, P.M. Zerwas, Hamburg 2002

[28] A. Denner, Fortsch. Phys. **41**, 307 (1993).

[29] A. Djouadi, W. Hollik and C. Jünger, Phys. Rev. D **55**, 6975 (1997); S. Kraml, H. Eberl, A. Bartl, W. Majerotto and W. Porod, Phys. Lett. B **386**, 175 (1996).

[30] S. Heinemeyer, W. Hollik and G. Weiglein, Eur. Phys. J. C **9**, 343 (1999) [arXiv:hep-ph/9812472]. S. Heinemeyer, W. Hollik and G. Weiglein, Comput. Phys. Commun. **124**, 76 (2000) [arXiv:hep-ph/9812320].

[31] K. Hagiwara *et al.* [Particle Data Group Collaboration], Phys. Rev. D **66**, 010001 (2002).

[32] A. Bartl, H. Eberl, S. Kraml, W. Majerotto and W. Porod, Eur. Phys. J. directC **2**, 6 (2000) [arXiv:hep-ph/0002115]. A. Finch, H. Nowak and A. Sopczak, arXiv:hep-ph/0211140.